PERGAMON

International Journal of Heat and Mass Transfer 45 (2002) 425–440

International Journal of HEAT and MASS TRANSFER

www.elsevier.com/locate/ijhmt

Transient thermal analysis of semitransparent composite layer with an opaque boundary

Ping-Yang Wang [a,*], Hui-Er Cheng [a], He-Ping Tan [b]

[a] *Institute of Engineering Thermophysics, Shanghai Jiaotong University, Shanghai 200030, China*
[b] *School of Energy Science and Engineering, Harbin Institute of Technology, Harbin 150001, China*

Received 20 January 2001

Abstract

Transient coupled radiative and conductive heat transfer in a two-layer, absorbing, emitting, and isotropically scattering non-gray slab is investigated by the ray tracing method in combination with Hottel's zonal method. One outer boundary is opaque, and another is semitransparent. The radiative energy transfer process in a semitransparent composite is divided into two sub-processes, one of which considers scattering, the other does not. The radiative transfer coefficients of the composite are deduced under specular and diffuse reflection and combined specular and diffuse reflection, respectively. The radiative heat source term is calculated by the radiative transfer coefficients. Temperature and heat flux are obtained by using the full implicit control-volume method in combination with the spectral band model. The method presented here needs only to disperse the space position, instead of the solid angle. A comparison with previous results shows that the results are more accurate.

1. Introduction

Semitransparent medium (STM) is widely applied to engineering, such as glass [1,2], ceramics [3], fibre [4], solid fuels [5] and so on. For a STM, energy can be directly transferred between the inside of the medium and its surroundings or opaque surface. The nature of the radiative transfer can provide a positive or negative internal heat source, and affect the temperature field and heat flux. For the STM at elevated temperatures, in high-temperature surroundings or subjected to large incident radiation, radiative heat transfer may be especially important. To obtain accurate temperature and heat flux in a STM, the radiative effect should be considered carefully as well as heat conduction.

Early studies of this subject were reviewed in detail by Viskanta and Anderson [6]. Recently, some researchers have focused on the coupled heat transfer in a two-layer or multi-layer planar STM. For example, based on the Galerkin method combined with a finite-difference method, Ho and Özisik [7,8] analyzed the transient coupled radiative and conductive heat transfer in a two-layer absorbing, isotropically scattering gray composite subjected to external radiation at one of its boundaries. The outer boundaries were diffuse and opaque. Spuckler and Siegel [9], and Siegel [10–12] investigated steady-state and transient temperature distribution in two-layer and multi-layer planar STM with diffuse reflective surface by using two-flux method in combination with Green's functions, and carefully studied the effects of isotropic scattering and refractivity of STM.

Transient temperatures were obtained for a single-layer, absorbing, and emitting STM [1] and for a single-layer isotropically scattering STM [13] by using the ray tracing method in combination with Hottel's zonal method [14] and the control-volume method, and the effects of the refractive index and the various radiative properties of surface and the thermal boundary conditions are included. In [15,16], this method was used to evaluate the internal radiative heat

* Corresponding author. Tel.: +86-021-62813617, +86-021-64473051.
E-mail address: wwpy@yahoo.com (P.-Y. Wang).

0017-9310/02/$ - see front matter
PII: S0017-9310(01)00143-0

Nomenclature

A_{k,T_i}	fractional spectral emissive power of spectral band k at nodal temperature T_i, $A_{k,T_i} = \int_{\Delta\lambda_k} I_{b,\lambda}(T_i)\,\mathrm{d}\lambda / \int_0^\infty I_{b,\lambda}(T_i)\,\mathrm{d}\lambda$
C_b	unit heat capacity of the bth layer, J m^{-3} K^{-1}
C_{21}	dimensionless unit heat capacity, $C_{21} = C_2/C_1$
$E_3(x)$	exponential integral function, $E_3(x) = \int_0^1 \exp(-x/\mu)\mu\,\mathrm{d}\mu$
$H_{n+1}[Y]$	function defined in Eq. (20)
H_1, H_2	convection–radiation parameter, $H_1 = h_1/(\sigma T_\mathrm{r}^3)$ and $H_2 = h_2/(\sigma T_\mathrm{r}^3)$
h_1, h_2	convective heat transfer coefficient at surfaces S_1 and S_2, respectively, W m^{-2} K^{-1}
k_{ie}, k_{iw}	harmonic mean thermal conductivity at the interface 'ie' and 'iw', W m^{-1} K^{-1}
L_b	thickness of each layer in the composite, m
L_t	total thickness of composite, $L_\mathrm{t} = L_1 + L_2$, m
M_b	number of control volumes in the bth layer
M_t	total number of control volumes in the composite, $M_\mathrm{t} = M_1 + M_2$
N_b	conduction–radiation parameter of the bth layer, $N_b = k_b/(4\sigma T_\mathrm{r}^3 L_\mathrm{t})$
NB	total number of spectral bands
n_b, n_i	refractive index of the bth layer and the ith control volume, respectively, $n_i = n_1$ when $i \leqslant M_1 + 1$, otherwise, $n_i = n_2$
n_s, n_h	smaller and larger refractive index, respectively
P_ref	quotient of specular reflection coefficients, Eq. (19)
$\widetilde{q}$	dimensionless heat flux, $\widetilde{q} = q/\sigma T_\mathrm{r}^4$
$\widetilde{q}^\mathrm{r}_{S_{-\infty}}, \widetilde{q}^\mathrm{r}_{S_{+\infty}}$	dimensionless external radiative fluxes incident at $x = 0$ and L_t, $\widetilde{q}^\mathrm{r}_{S_{-\infty}} = \sigma T^4_{S_{-\infty}}/(\sigma T_\mathrm{r}^4)$, $\widetilde{q}^\mathrm{r}_{S_{+\infty}} = \sigma T^4_{S_{+\infty}}/(\sigma T_\mathrm{r}^4)$
$q^\mathrm{r}, q^\mathrm{cd}, q^\mathrm{cv}$	radiative, conductive and convective heat fluxes, respectively, W m^{-2}
q^t	total heat flux, $q^\mathrm{t} = q^\mathrm{cd} + q^\mathrm{r}$
$q^\mathrm{r}_{S_1}, q^\mathrm{r}_{S_2}$	radiative heat fluxes at surface S_1 and S_2
S_1, S_2	boundary surfaces (Fig. 1)
S_P	internal interface of two layers (Fig. 1)
$S_{-\infty}, S_{+\infty}$	black surfaces denoting the black environment (Fig. 1)
$(S_hS_c)_k,\ (S_hV_j)_k,\ (V_iV_j)_k$	radiation transfer coefficients of surface vs. surface, surface vs. volume and volume vs. volume in non-scattering media relative to the spectral band $k(\Delta\lambda_k)$
$[S_hS_c]_k,\ [S_hV_j]_k,\ [V_iV_j]_k$	radiation transfer coefficients of surface vs. surface, surface vs. volume and volume vs. volume in isotropically scattering media relative to the spectral band $k(\Delta\lambda_k)$
T_i	absolute temperature of control volume i, K
$TI_1, TI_2, \ldots$	fraction of radiative intensity transmitted through an interface (Fig. 3)
T_{g1}, T_{g2}	gas temperatures for convection at $X = 0$ and $X = 1$, respectively, K (Fig. 1)
$\widetilde{T}_{g1}, \widetilde{T}_{g2}$	dimensionless gas temperatures $\widetilde{T}_{g1} = T_{g1}/T_\mathrm{r}$, $\widetilde{T}_{g2} = T_{g2}/T_\mathrm{r}$
T_r	reference temperature or uniform initial temperature, K
T_{S_1}, T_{S_2}	temperatures of the boundary surfaces S_1 and S_2, respectively, K
$\widetilde{T}_{S_1}, \widetilde{T}_{S_2}$	dimensionless temperatures $\widetilde{T}_{S_1} = T_{S_1}/T_\mathrm{r}$, $\widetilde{T}_{S_2} = T_{S_2}/T_\mathrm{r}$
$T_{S_{-\infty}},\ T_{S_{+\infty}}$	temperatures of the black environment, K (Fig. 1)
t	physical time, s
$\widetilde{t}$	dimensionless time, $\widetilde{t} = (4\sigma T_\mathrm{r}^3/C_1L_\mathrm{t})t$
$\widetilde{t}_\mathrm{s}$	steady-state dimensionless time
Δt	time interval, s
x	coordinate in direction perpendicular to layer interface, m; $X = x/L_\mathrm{t}$
Δx	spatial interval, m (Fig. 1)
$x_{1,1_i} \ldots$	distance of ray transfer between both subscripts, m (Fig. 1)
z	distance of ray transfer, m
Greek symbols	
γ_{g1}, γ_{1g}	transmissivity at surface S_1
γ_{bP}	transmissivity at internal interface (Fig. 1)

δ	dimensionless thickness of the 1st layer $\delta = L_1/L_t$
$\varepsilon_{g2}, \varepsilon_{2g}$	emissivities at boundary surfaces (Fig. 1)
η_i	$1-\omega_i$, when $i \leqslant M_1+1$, $\omega_i = \omega_1$, otherwise $\omega_i = \omega_2$
θ, φ	angle of reflection, incidence or refraction, respectively
$\kappa_{b,k}$	extinction coefficients of layer b, m^{-1}
λ	wavelength, m
μ	direction cosine, $\mu = \cos(\theta)$
$\mu_{1g}, \mu_{2g}, \mu_{21}$	critical direction cosine
$\rho_{gb}, \rho_{bg}, \rho_{bP}$	reflectivities at interfaces
$\rho_{s\to h}, \rho_{h\to s}$	reflectivities, subscript '$s \to h$' denotes radiation from a smaller to a larger refractive index and subscript '$h \to s$' from a larger to a smaller refractive index
σ	Stefan–Boltzmann constant, W m^{-2} K^{-4}
$\sigma_{s,k}$	spectral scattering coefficient, m^{-1}
$\tau_{b,k}$	spectral optical thickness of layer b
Φ_i^r	radiative heat source of control volume i
$\omega_{b,k}$	spectral single-scattering albedo of layer b
Subscripts	
a	absorbed quotient in the overall attenuated radiative energy
b	layer index: $b = 1$ in 1st layer; $b = 2$ in 2nd layer
bP	from layer b to the interface of two layers
c, h	index, $c, h = -\infty, 2$
gb, bg	'gb' denotes from gas to layer b and 'bg' denotes form layer b to gas
ie, iw	right and left interface of control volume i (Fig. 1)
k	relative to spectral band k
Superscripts	
d, s	diffuse and specular reflection, respectively
s + d	combined specular and diffuse reflection
$m, m+1$	time step

source and to solve the transient energy equation for a two-layer isotropically scattering STM with the semitransparent or the opaque outer boundaries, and the results for many conditions are obtained. The objective of present paper is to extend the method to study the transient coupled radiation and conduction in a two-layer isotropically scattering STM with one opaque outer boundary and one semitransparent outer boundary and the semitransparent internal interface. Each layer has different radiative properties and different refractive index, and the effects of single-scattering albedo, reflective characteristics, conduction–radiation parameter, and emissivity on the temperature distribution and heat flux are included.

2. Analysis

2.1. Physical model and governing equations

The analysis is for an absorbing, emitting, and isotropically scattering composite composed of a two-layer composite planar STM. As shown in Fig. 1, the composite layer is between two black surfaces ($S_{-\infty}$ and $S_{+\infty}$), whose temperatures are $T_{S_{-\infty}}$ and $T_{S_{+\infty}}$, respectively. Boundary surface S_2 is opaque, and boundary surface S_1 and internal interface S_P are semitransparent. The 1st layer is divided into M_1 control volumes along its thickness, and the 2nd layer is divided into M_2 control volumes, and the total number of nodal is $M_t = M_1 + M_2 + 2$. 1_i and 2_i are used to represent the ith node in the 1st layer and the 2nd layer, respectively. 1_i and 2_i are shortened to i in the following equations except for radiative transfer coefficient (RTC), i.e., when $i \leqslant M_1 + 1$, i represents the ith node in the 1st layer and the subscript in the equation is $b = 1$; otherwise i represents the $(i - M_1 - 1)$th node in the 2nd layer and $b = 2$. Considering transient coupled radiation and conduction, between the time intervals t $(= m\Delta t)$ and $t + \Delta t$ $(= [m+1]\Delta t)$, the fully implicit discrete energy equation of control volume i is obtained as

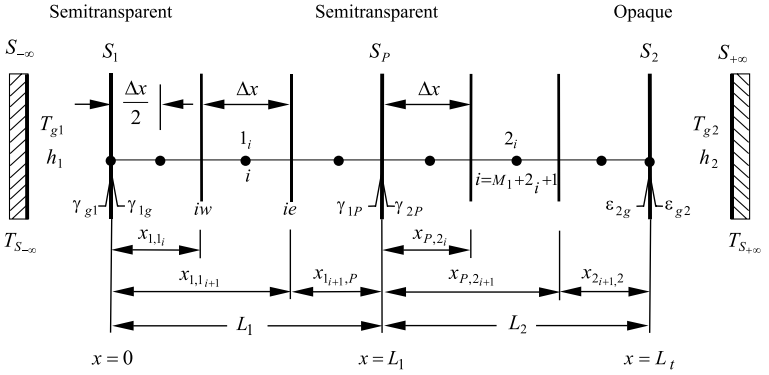

Fig. 1. The zonal discretization model of a two-layer planar composite medium.

$$C_b\Delta x\frac{T_i^{m+1}-T_i^m}{\Delta t}=\frac{k_{ie}^{m+1}\left(T_{i+1}^{m+1}-T_i^{m+1}\right)+k_{iw}^{m+1}\left(T_{i-1}^{m+1}-T_i^{m+1}\right)}{\Delta x}+\Phi_i^{\mathrm{r},m+1}. \tag{1}$$

2.2. Radiative heat source

The key to solving the transient discrete energy equation is to solve the local radiative heat source term (Φ_i^{r}). As far as one-dimensional problem is concerned, the radiative heat source of control volume i is equal to the difference of radiative flux densities between its two interfaces [13]:

$$\Phi_i^{\mathrm{r}}=q_{ie}^{\mathrm{r}}(T)-q_{iw}^{\mathrm{r}}(T)=q_{ie}^{\mathrm{r}}(T)-q_{(i-1)e}^{\mathrm{r}}(T),\quad 2\leqslant i\leqslant M_{\mathrm{t}}+1. \tag{2}$$

For semitransparent surface S_1, opaque surface S_2, q_{ie}^{r} can be written as

$$\begin{aligned}q_{ie}^{\mathrm{r}}=\sigma\sum_{k=1}^{\mathrm{NB}}\Bigg\{&n_{2,k}^2[S_2S_{-\infty}]_kA_{k,T_{S_2}}T_{S_2}^4-[S_{-\infty}S_2]_kA_{k,T_{S_{-\infty}}}T_{S_{-\infty}}^4+\sum_{j=2}^{i}\left[n_{2,k}^2\left[S_2V_j\right]_kA_{k,T_{S_2}}T_{S_2}^4-n_{j,k}^2\left[V_jS_2\right]_kA_{k,T_j}T_j^4\right]\\&+\sum_{j=i+1}^{M_t+1}\sum_{l=2}^{i}\left[n_{j,k}^2\left[V_jV_l\right]_kA_{k,T_j}T_j^4-n_{l,k}^2\left[V_lV_j\right]_kA_{k,T_l}T_l^4\right]+\sum_{j=i+1}^{M_t+1}\left[n_{j,k}^2\left[V_jS_{-\infty}\right]_kA_{k,T_j}T_j^4-\left[S_{-\infty}V_j\right]_kA_{k,T_{S_{-\infty}}}T_{S_{-\infty}}^4\right]\Bigg\},\\&2\leqslant i\leqslant M_{\mathrm{t}}.\end{aligned} \tag{3}$$

When $i=1$ and $i=M_{\mathrm{t}}+1$, the radiative heat flux densities of boundary surfaces $q_{S_1}^{\mathrm{r}}$ and $q_{S_2}^{\mathrm{r}}$ are given as follows:

$$\begin{aligned}q_{S_1}^{\mathrm{r}}&=q_{2w}^{\mathrm{r}}\\&=\sigma\sum_{k=1}^{\mathrm{NB}}\left\{n_{2,k}^2[S_2S_{-\infty}]_kA_{k,T_{S_2}}T_{S_2}^4-[S_{-\infty}S_2]_kA_{k,T_{S_{-\infty}}}T_{S_{-\infty}}^4+\sum_{j=2}^{M_t+1}\left[n_{j,k}^2\left[V_jS_{-\infty}\right]_kA_{k,T_j}T_j^4-\left[S_{-\infty}V_j\right]_kA_{k,T_{S_{-\infty}}}T_{S_{-\infty}}^4\right]\right\},\end{aligned} \tag{4a}$$

$$\begin{aligned}q_{S_2}^{\mathrm{r}}&=q_{(M_t+1)e}^{\mathrm{r}}\\&=\sigma\sum_{k=1}^{\mathrm{NB}}\left\{n_{2,k}^2[S_2S_{-\infty}]_kA_{k,T_{S_2}}T_{S_2}^4-[S_{-\infty}S_2]_kA_{k,T_{S_{-\infty}}}T_{S_{-\infty}}^4+\sum_{j=2}^{M_t+1}\left[n_{2,k}^2\left[S_2V_j\right]_kA_{k,T_{S_2}}T_{S_2}^4-n_{j,k}^2\left[V_jS_2\right]_kA_{k,T_j}T_j^4\right]\right\}.\end{aligned} \tag{4b}$$

2.3. Boundary and initial conditions

For semitransparent surface S_1, radiative energy can be directly transferred from the surroundings to the interior of the composite, so that the conduction and convection conditions at S_1 is

$$h_1(T_{S_1}-T_{g1})=2k_{2w}(T_2-T_{S_1})/\Delta x,\quad x=0. \tag{5a}$$

For opaque surface S_2, there is radiative and conductive heat transfer between S_2 and the interior of the composite, and between S_2 and the surroundings, so the boundary condition is

$$q^{r}_{S_2} + 2k^{m+1}_{(M_t+1)e}(T_{S_2} - T_{M_t+1})/\Delta x = \sigma \sum_{k=1}^{NB} \varepsilon_{2,k}\left[A_{k,T_{S_{+\infty}}} T^4_{S+\infty} - A_{k,T_{S_2}} T^4_{S_2}\right] + h_2(T_{g2} - T_{S_2}), \quad x = L_t, \tag{5b}$$

where $q^{r}_{S_2}$ is given by Eq. (4b). The reflection and refraction at interface S_P are considered in RTC.

If convective heat transfer coefficients h_1 and h_2 in Eqs. (5a) and (5b) approach infinity, the surface temperature is equal to that of the surroundings, i.e., $T_{S_1} = T_{g1}$ and $T_{S_2} = T_{g2}$, then Eqs. (5a) and (5b) become first kind boundary conditions. If h_1 is finite but h_2 is infinite, Eqs. (5a) and (5b) become mixed boundary conditions, i.e., a first kind boundary condition at surface S_2 and a third kind at surface S_1.

Although the initial condition for the results given here is a uniform temperature distribution, the method is valid for an arbitrary initial temperature distribution.

3. Radiative transfer coefficient (RTC)

RTC of a surface or a control-volume element i vs. element j is defined as the quotient of the radiative energy absorbed by element j in the transfer process of the radiative energy emitted by element i. For a scattering STM, the transfer process includes:

1. the radiative energy reaching element j directly,
2. the reflection by surfaces once or many times,
3. the scattering by the medium once or many times.

The transfer process of radiative energy in a scattering STM can be divided into two sub-processes according to the transfer mechanism. That is,

1. Only the absorption, emission and reflection of the STM are considered, but not its scattering.
2. Only scattering is considered according to the scattering mechanism – for isotropic scattering, the radiative intensity scattered by element j is distributed uniformly. Such distribution is equivalent to the spacial distribution of the radiative intensity emitted by element j.

3.1. RTC without considering scattering

3.1.1. RTC for specular reflection

By using the energy transfer relations of Hottel's zonal method [14] between surfaces and control volumes, between control volumes and control volumes, and the geometric relations in Fig. 1, under specular reflection, the process of deducing RTC $(S_{-\infty}S_2)^s_k$ is taken, here, as an example.

To form a more concise notation, four functions are defined [15]:

$$FT_{b,k}(z) = \exp(-\kappa_{b,k} z/\mu_b), \tag{6a}$$

$$FJ_{b,k} = \rho_{bP}\rho_{bg} FT_{b,k}(2L_b), \tag{6b}$$

$$FJ_k = \left[\gamma_{1P}\gamma_{2P}\rho_{1g}\rho_{2g} FT_{1,k}(2L_1) FT_{2,k}(2L_2)\right]/[(1 - FJ_{1,k})(1 - FJ_{2,k})], \tag{6c}$$

$$FA_{b,k} = 1 - FT_{b,k}(\Delta x). \tag{6d}$$

Under specular reflection, the incident angle of a ray is equal to the reflective angle. Therefore, the expression for radiative intensity attenuation along the path of a ray emitted at an arbitrary angle can be determined by tracing this ray. Then the RTC considering multiple reflection for an absorbing, emitting STM can be calculated by integrating in hemispheric space. As shown in Fig. 2, the unit radiative intensity transmitted through the upper surface into the STM is absorbed by the medium and the opaque surface, and transmitted through the semitransparent surface, and, in the end, attenuated to zero. During this process, the total radiative intensity reaching the lower surface will be [13] $FT_{b,k}(L_b)/(1 - FJ_{b,k})$ for Process 1

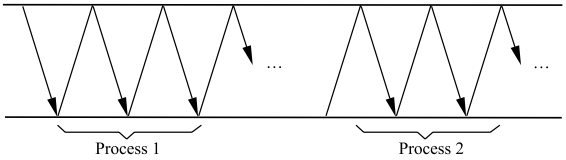

Fig. 2. Diagram of the radiative propagating in a single STM for specular boundaries.

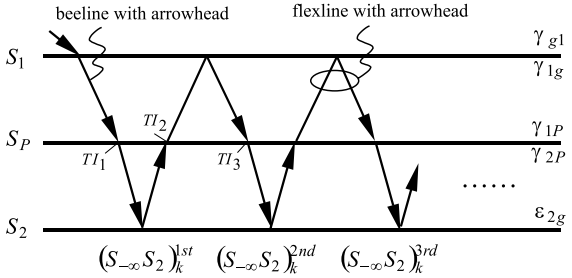

Fig. 3. Diagram of equivalent radiative propagating in a two-layer STM for specular boundaries.

and $FT_{b,k}(2L_b)/(1-FJ_{b,k})$ for Process 2, where the subscript 'b' denotes the radiation transfer process occurring in the bth layer. Fig. 3 provides the equivalent radiative propagating in a two-layer STM with specular surfaces, and the beeline and flexline with arrowhead within each layer denote Process 1 and Process 2 of Fig. 2, respectively. As shown in Fig. 3, the unit radiative intensity emitted by surroundings $S_{-\infty}$ and transmitted into the composite attenuates to zero due to the processes occurring in the first layer. Part of the radiative intensity, denoted by TI_1, is transmitted into the second layer through interface S_P, and the rest is absorbed by the first layer medium and transmitted into the surroundings. TI_1 can be divided into three parts: the first part, denoted by TI_2, comes back to the first layer through interface S_P; the second part, denoted by $(S_{-\infty}S_2)_k^{1st}$, is absorbed by opaque surface S_2 and is called first-order absorption,

$$(S_{-\infty}S_2)_k^{1st} = n_{2,k}^2 \frac{\gamma_{g1}\gamma_{1P}\varepsilon_{2g}FT_{1,k}(L_1)FT_{2,k}(L_2)}{(1-FJ_{1,k})(1-FJ_{2,k})}, \tag{7a}$$

the last part is absorbed by the control volumes of the second layer. For TI_2, the part denoted by TI_3 is transmitted into the second layer. Just as for TI_1, TI_3 can also be divided into three parts. Thus, the part denoted by $(S_{-\infty}S_2)_k^{2nd}$ is absorbed by opaque surface S_2 and is called second-order absorption, or

$$(S_{-\infty}S_2)_k^{2nd} = n_{2,k}^2 \frac{\gamma_{g1}\gamma_{1P}\varepsilon_{2g}FT_{1,k}(L_1)FT_{2,k}(L_2)}{(1-FJ_{1,k})(1-FJ_{2,k})}(FJ_k)^1. \tag{7b}$$

By analogy, third-order absorption is

$$(S_{-\infty}S_2)_k^{3rd} = n_{2,k}^2 \frac{\gamma_{g1}\gamma_{1P}\varepsilon_{2g}FT_{1,k}(L_1)FT_{2,k}(L_2)}{(1-FJ_{1,k})(1-FJ_{2,k})}(FJ_k)^2, \tag{7c}$$

and the $(n+1)$th-order absorption is:

$$(S_{-\infty}S_2)_k^{(n+1)th} = n_{2,k}^2 \frac{\gamma_{g1}\gamma_{1P}\varepsilon_{2g}FT_{1,k}(L_1)FT_{2,k}(L_2)}{(1-FJ_{1,k})(1-FJ_{2,k})}(FJ_k)^n. \tag{7d}$$

According to the above analysis, in the entire transfer process, in which the radiative intensity emitted by $S_{-\infty}$ comes into the composite medium, and then is attenuated to zero, the total radiative intensity absorbed by opaque boundary surface S_2 is the sum of the geometric progression represented by Eq. (7d). Then RTC $(S_{-\infty}S_2)_k^s$ can be calculated by integrating the total radiative intensity over a hemisphere as

$$\begin{aligned}(S_{-\infty}S_2)_k^s &= 2\int_{\mu_{2g}}^1 \left[(S_{-\infty}S_2)_k^{1st} + (S_{-\infty}S_2)_k^{2nd} + (S_{-\infty}S_2)_k^{3rd} + \cdots\right]\mu_2\,\mathrm{d}\mu_2 \\ &= 2n_{2,k}^2\int_{\mu_{2g}}^1 \frac{\gamma_{g1}\gamma_{1P}\varepsilon_{2g}FT_{1,k}(L_1)FT_{2,k}(L_2)}{(1-FJ_{1,k})(1-FJ_{2,k})(1-FJ_k)}\mu_2\,\mathrm{d}\mu_2.\end{aligned} \tag{7e}$$

For specular reflection, the RTCs of the composite with one semitransparent outer boundary and one opaque outer boundary have the following reciprocal relationships:

$$\begin{aligned}&\gamma_{2P}\gamma_{1g}(S_{-\infty}S_2)_k^s = n_{2,k}^2\gamma_{1P}\gamma_{g1}(S_2S_{-\infty})_k^s, && (S_{-\infty}V_{1_j})_k^s\gamma_{1g} = n_{1,k}^2\gamma_{g1}(V_{1_j}S_{-\infty})_k^s,\\ &n_{2,k}^2\gamma_{1P}(S_2V_{1_j})_k^s = n_{1,k}^2\gamma_{2P}(V_{1_j}S_2)_k^s, && (S_{-\infty}V_{2_j})_k^s\gamma_{2P}\gamma_{1g} = n_{2,k}^2\gamma_{1P}\gamma_{g1}(V_{2_j}S_{-\infty})_k^s,\\ &(S_2V_{2_j})_k^s = (V_{2_j}S_2)_k^s, && n_{1,k}^2\gamma_{2P}(V_{1_i}V_{2_j})_k^s = n_{2,k}^2\gamma_{1P}(V_{2_j}V_{1_i})_k^s,\\ &(V_{1_i}V_{1_j})_k^s = (V_{1_j}V_{1_i})_k^s, && (V_{2_i}V_{2_j})_k^s = (V_{2_j}V_{2_i})_k^s.\end{aligned} \tag{8}$$

So, one of each pair of the RTCs except for $(S_{-\infty}S_2)_k^s$ is given by Eqs. (9)–(15):

$$\left(S_{-\infty}V_{1_j}\right)_k^s = 2\gamma_{g1}n_{1,k}^2\int_{\mu_{1g}}^1 FA_{1,k}\left\{\frac{FT_{1,k}(x_{1,1_j})+\rho_{1P}FT_{1,k}(L_1+x_{P,1_{j+1}})}{1-FJ_{1,k}} + \frac{\gamma_{1P}\gamma_{2P}\rho_{2g}FT_{1,k}(L_1)FT_{2,k}(2L_2)\left[FT_{1,k}(x_{P,1_{j+1}})+\rho_{1g}FT_{1,k}(L_1+x_{1,1_j})\right]}{(1-FJ_{1,k})^2(1-FJ_{2,k})(1-FJ_k)}\right\}\mu_1\,\mathrm{d}\mu_1, \tag{9}$$

$$\left(S_2V_{1_j}\right)_k^s = 2\varepsilon_{2g}n_{1,k}^2\int_0^1 FA_{1,k}\frac{\gamma_{2P}FT_{2,k}(L_2)\left[FT_{1,k}(x_{P,1_{j+1}})+\rho_{1g}FT_{1,k}(L_1+x_{1,1_j})\right]}{(1-FJ_{1,k})(1-FJ_{2,k})(1-FJ_k)}\mu_1\,\mathrm{d}\mu_1, \tag{10}$$

$$\left(S_{-\infty}V_{2_j}\right)_k^s = 2\gamma_{g1}n_{2,k}^2\int_{\mu_{2g}}^1 FA_{2,k}\frac{\gamma_{1P}FT_{1,k}(L_1)\left[FT_{2,k}(x_{P,2_j})+\rho_{2g}FT_{2,k}(L_2+x_{2,2_{j+1}})\right]}{(1-FJ_{1,k})(1-FJ_{2,k})(1-FJ_k)}\mu_2\,\mathrm{d}\mu_2, \tag{11}$$

$$\left(S_2V_{2_j}\right)_k^s = 2\varepsilon_2\int_0^1 FA_{2,k}\left\{\frac{FT_{2,k}(x_{2,2_{j+1}})+\rho_{2P}FT_{2,k}(L_2+x_{P,2_j})}{(1-FJ_{2,k})} + \frac{\gamma_{2P}\gamma_{1P}\rho_{1g}FT_{2,k}(L_2)FT_{1,k}(2L_1)\left[FT_{2,k}(x_{P,2_j})+\rho_{2g}FT_{2,k}(L_2+x_{2,2_{j+1}})\right]}{(1-FJ_{2,k})^2(1-FJ_{1,k})(1-FJ_k)}\right\}\mu_2\,\mathrm{d}\mu_2, \tag{12}$$

$$\left(V_{1_i}V_{2_j}\right)_k^s = \int_{\mu_{21}}^1 \frac{2n_{2,k}^2FA_{1,k}FA_{2,k}\gamma_{1P}}{(1-FJ_{1,k})(1-FJ_{2,k})(1-FJ_k)}\left[FT_{1,k}(x_{1_{i+1},P})+\rho_{1g}FT_{1,k}(x_{1_i,1}+L_1)\right] \times\left[FT_{2,k}(x_{P,2_j})+\rho_{2g}FT_{2,k}(L_2+x_{2,2_{j+1}})\right]\mu_2\,\mathrm{d}\mu_2, \tag{13}$$

$$\left(V_{1_i}V_{1_j}\right)_k^s = R_{1,k}+2\int_0^1\frac{FA_{1,k}^2}{1-FJ_{1,k}}\left\{\rho_{1g}FT_{1,k}(x_{1_i,1}+x_{1,1_j})+\rho_{1g}\rho_{1P}FT_{1,k}(x_{1_i,1}+L_1+x_{P,1_{j+1}}) + \rho_{1g}\rho_{1P}FT_{1,k}(x_{1_{i+1},P}+L_1+x_{1,1_j})+\rho_{1P}FT_{1,k}(x_{1_{i+1},P}+x_{P,1_{j+1}}) + \frac{\left[\rho_{1g}FT_{1,k}(x_{1_i,1}+L_1)+FT_{1,k}(x_{1_{i+1},P})\right]\left[FT_{1,k}(x_{P,1_{j+1}})+\rho_{1g}FT_{1,k}(L_1+x_{1,1_j})\right]}{(1-FJ_{1,k})(1-FJ_{2,k})(1-FJ_k)/\left[\gamma_{1P}\rho_{2g}\gamma_{2P}FT_{2,k}(2L_2)\right]}\right\}\mu_1\,\mathrm{d}\mu_1, \tag{14}$$

$$\left(V_{2_i}V_{2_j}\right)_k^s = R_{2,k}+2\int_0^1\frac{FA_{2,k}^2}{1-FJ_{2,k}}\left\{\rho_{2P}FT_{2,k}(x_{2_i,P}+x_{P,2_j})+\rho_{2g}\rho_{2P}FT_{2,k}(x_{2_{i+1},2}+L_2+x_{P,2_j}) +\rho_{2g}FT_{2,k}(x_{2_{i+1},2}+x_{2,2_{j+1}})+\rho_{2g}\rho_{2P}FT_{2,k}(x_{2_i,P}+L_2+x_{2,2_{j+1}}) +\frac{\left[FT_{2,k}(x_{2_i,P})+\rho_{2g}FT_{2,k}(x_{2_{i+1},2}+L_2)\right]\left[FT_{2,k}(x_{P,2_j})+\rho_{2g}FT_{2,k}(L_2+x_{2,2_{j+1}})\right]}{(1-FJ_{2,k})(1-FJ_{1,k})(1-FJ_k)/\left[\gamma_{2P}\gamma_{1P}\rho_{1g}FT_{1,k}(2L_1)\right]}\right\}\mu_2\,\mathrm{d}\mu_2. \tag{15}$$

The RTCs of surroundings $S_{-\infty}$ and opaque surfaces S_2 have no reciprocal relationship, and are given as

$$(S_{-\infty}S_{-\infty})_k^s = \rho_{g1}+2n_{1,k}^2\gamma_{g1}\gamma_{1g}\int_{\mu_{1g}}^1\left\{\frac{\rho_{1P}FT_{1,k}(2L_1)}{1-FJ_{1,k}}+\frac{\gamma_{1P}\rho_{2g}\gamma_{2P}FT_{1,k}(2L_1)FT_{2,k}(2L_2)}{(1-FJ_{1,k})^2(1-FJ_{2,k})(1-FJ_k)}\right\}\mu_1\,\mathrm{d}\mu_1, \tag{16}$$

$$(S_2S_2)_k^s = 2\varepsilon_2\varepsilon_2\int_0^1\left\{\frac{\rho_{2P}FT_{2,k}(2L_2)}{1-FJ_{2,k}}+\frac{\rho_{1g}\gamma_{1P}\gamma_{2P}FT_{2,k}(2L_2)FT_{1,k}(2L_1)}{(1-FJ_{2,k})^2(1-FJ_{1,k})(1-FJ_k)}\right\}\mu_2\,\mathrm{d}\mu_2, \tag{17}$$

where

$$R_{b,k} = 4\kappa_{b,k}\Delta x-2[1-2E_3(\kappa_{b,k}\Delta x)]\quad(i=j),\qquad R_{b,k}=2\int_0^1 FA_{b,k}^2FT_{b,k}(x_{b_i,b_j})\mu_b\,\mathrm{d}\mu_b\quad(i\neq j).$$

A limiting condition, $n_1\leqslant n_2$, is implied in the above equations, so that the critical angles are:

$$\mu_{1g}=\sqrt{1-(1/n_1)^2},\quad \mu_{2g}=\sqrt{1-(1/n_2)^2},\quad\text{and}\quad \mu_{21}=\sqrt{1-(n_1/n_2)^2}.$$

Considering the total reflection, the following limiting conditions must be met: if $\mu_2 \leqslant \mu_{21}$, then $\rho_{2P} = 1$, $\gamma_{2P} = 0$; if $\mu_{21} \leqslant \mu_2 \leqslant \mu_{2g}$ or $0 \leqslant \mu_1 \leqslant \mu_{1g}$, then $\rho_{1P} = 1$.

3.1.2. RTC for diffuse reflection

When RTC is deduced by the ray tracing method for specular reflection, the radiative intensity is determined at first, then RTC can be calculated by integrating the total radiative intensity. For diffuse reflection, the direct radiative transfer coefficient (DRTC) is needed to calculate RTC, but the tracing process of radiative energy is the same as that for specular reflection, so it is omitted here. The RTC equations and the reciprocity relationships for diffuse reflection are provided in Appendix A.

3.1.3. RTC for combined specular and diffuse reflection

RTC equations for combined specular and diffuse reflection are obtained, here, by a linear sum of the RTC equations for specular reflection and that for diffuse reflection. As shown in Eqs. (18a)–(18d)

$$(S_hS_c)_k^{s+d} = P_{ref} \times (S_hS_c)_k^{s} + (1 - P_{ref}) \times (S_hS_c)_k^{d} \quad (S_h, S_c = S_{-\infty}, S_2), \tag{18a}$$

$$\left(S_hV_j\right)_k^{s+d} = P_{ref} \times \left(S_hV_j\right)_k^{s} + (1 - P_{ref}) \times \left(S_hV_j\right)_k^{d} \quad (S_h = S_{-\infty}, S_2), \tag{18b}$$

$$(V_iS_c)_k^{s+d} = P_{ref} \times (V_iS_c)_k^{s} + (1 - P_{ref}) \times (V_iS_c)_k^{d} \quad (S_c = S_{-\infty}, S_2), \tag{18c}$$

$$\left(V_iV_j\right)_k^{s+d} = P_{ref} \times \left(V_iV_j\right)_k^{s} + (1 - P_{ref}) \times \left(V_iV_j\right)_k^{d}, \tag{18d}$$

where P_{ref} is the quotient of specular reflection coefficients.

$$P_{ref} = (\rho_{g1}^{s} + \rho_{1g}^{s} + \cdots)/(\rho_{g1}^{s} + \rho_{1g}^{s} + \cdots + \rho_{g1}^{d} + \rho_{1g}^{d} + \cdots). \tag{19}$$

RTC for a two-layer, absorbing, emitting, and isotropically scattering STM with both semitransparent boundaries and both opaque boundaries were provided in [15,16], respectively.

3.2. RTC considering isotropic scattering

When the effect of scattering is considered, the fractions of radiative energy represented by RTCs (S_hS_c), (S_hV_j), (V_iV_j) will be redistributed. For convenience's sake, subscript 'k' and superscripts 's', 'd' and 's + d' are omitted in the following equations. Omission is necessary because, when isotropic scattering is considered, the derivational process and the final form of the RTC equation are the same regardless of whether the medium is spectral or gray, and whether there is specular, diffuse or combined specular and diffuse reflection.

Taking $[V_iV_j]$ as an example, the derivation of RTC equation, considering isotropic scattering, is given here. A midterm function $H_{n+1}[Y]$ is defined:

$$H_{n+1}[Y] = \omega_{l_2}\left\{\sum_{l_3=2}^{M_t+1}(V_{l_2}V_{l_3})\omega_{l_3}\left\{\sum_{l_4=2}^{M_t+1}(V_{l_3}V_{l_4})\omega_{l_4} \times \cdots \times \left[\sum_{l_{n+1}=2}^{M_t+1}(V_{l_n}V_{l_{n+1}})\omega_{l_{n+1}}Y\right]\right\}\right\}. \tag{20}$$

After first-order scattering, for the fraction of energy transfer denoted by RTC$\left(V_iV_j\right)$, only η_j is absorbed, i.e.,

$$\left[V_iV_j\right]_a^{1st} = (V_iV_j)\eta_j. \tag{21a}$$

After second-order scattering,

$$\left[V_iV_j\right]_a^{2nd} = \left[V_iV_j\right]_a^{1st} + \sum_{l_2=1}^{M_t+1}(V_iV_{l_2})\omega_{l_2}(V_{l_2}V_j)\eta_j = \left[V_iV_j\right]_a^{1st} + \sum_{l_2=1}^{M_t+1}(S_{-\infty}V_{l_2})H_2\left[(V_{l_2}V_j)\eta_j\right]. \tag{21b}$$

After third-order scattering,

$$\left[V_iV_j\right]_a^{3rd} = \left[V_iV_j\right]_a^{2nd} + \sum_{l_2=1}^{M_t+1}(V_iV_{l_2})H_3\left[(V_{l_3}V_j)\eta_j\right]. \tag{21c}$$

Similarly, after the $(n+1)$th-order scattering, each RTC is given by

$$\left[V_iV_j\right]_a^{(n+1)th} = \left[V_iV_j\right]_a^{nth} + \sum_{l_2=2}^{M_t+1}(V_iV_{l_2})H_{n+1}\left[(V_{l_{n+1}}V_j)\eta_j\right], \tag{22}$$

$$\left[S_h V_j\right]_a^{(n+1)\text{th}} = \left[S_h V_j\right]_a^{n\text{th}} + \sum_{l_2=2}^{M_l+1} (S_h V_{l_2}) H_{n+1} \left[(V_{l_{n+1}} V_j)\eta_j\right], \tag{23}$$

$$\left[V_i S_c\right]_a^{(n+1)\text{th}} = \left[V_i S_c\right]_a^{n\text{th}} + \sum_{l_2=2}^{M_l+1} (V_i V_{l_2}) H_{n+1} \left[(V_{l_{n+1}} S_c)\right], \tag{24}$$

$$\left[S_h S_c\right]_a^{(n+1)\text{th}} = \left[S_h S_c\right]_a^{n\text{th}} + \sum_{l_2=2}^{M_l+1} (S_h V_{l_2}) H_{n+1} \left[(V_{l_{n+1}} S_c)\right]. \tag{25}$$

3.3. Determination of reflectivity

Reflectivity ρ of a semitransparent surface can be obtained from Fresnel's equations [17]. When radiation passes into a material of a larger refractive index, reflectivity $\rho_{s\to h}$ is

$$\rho_{s\to h} = \int_0^{\pi/2} \left\{ \left[\frac{n_h \cos(\varphi) - n_s \cos(\theta)}{n_h \cos(\varphi) + n_s \cos(\theta)}\right]^2 + \left[\frac{n_s \cos(\varphi) - n_h \cos(\theta)}{n_s \cos(\varphi) + n_h \cos(\theta)}\right]^2 \right\} \sin(\theta)\cos(\theta)\, \mathrm{d}\theta, \tag{26a}$$

where θ is the incidence angle, φ is the refractive angle, and $\varphi = \arcsin[n_s \sin(\theta)/n_h]$. When radiation goes from a larger to a smaller n value, reflectivity $\rho_{h\to s}$ is given by [18] as

$$\rho_{h\to s} = 1 - (n_s/n_h)^2 + \rho_{\mathrm{s}\to\mathrm{h}}\, (n_s/n_h)^2, \tag{26b}$$

where '$1 - (n_s/n_h)^2$' is caused by total reflection. For a specular surface, the total reflection is considered in the RTCs. Therefore, $\rho^s_{h\to s}$ becomes

$$\rho^s_{h\to s} = \rho^s_{s\to h}\, (n_s/n_h)^2. \tag{26c}$$

For a diffuse surface, it is assumed that each bit of roughness acts as a smooth facet [17] and total reflection is considered in the reflectivity so that the reflectivity can be directly obtained from Eqs. (26a) and (26b).

4. Verification of the computational method

By far, the research for coupled radiation–conduction in a two-layer STM with one semitransparent outer boundary and one opaque outer boundary were not found in the open literature. To partially validate the present solution, the results of the coupled radiation–conduction in [8] for a two-layer STM with both opaque outer boundaries and [9,10] for a two-layer STM with both semitransparent outer boundaries are used for comparing with the present results.

The steady-state dimensionless temperatures and heat fluxes here for a two-layer STM with both opaque outer boundaries are compared with those in [8]. The input parameters are: both of the boundary surfaces are black, $\varepsilon_{1g} = \varepsilon_{2g} = 1$; the boundary conditions are the first kind, $\widetilde{T}_{S_1} = 0.5$, $\widetilde{T}_{S_2} = 1.0$; the radiation–conduction parameters of both layers are the same, $N_1 = N_2 = N$; and the reflection is ignored at the internal interface. The results are shown in Table 1. Whether conduction ($N = 1.0$) or radiation ($N = 0.01$) is dominant, the steady-state temperature and net heat flux using the present method are in good agreement with the results of Ho and Özisik [8]. The maximum relative error of temperature is 0.027%, and that of net heat flux is 0.061%.

Under both semitransparent outer boundaries and diffuse reflection, Figs. 4(a) and (b) provide a comparison with an exact numerical solution [9] and an approximate solution using Green's function and the two-flux method [10]. Fig. 4(a) has the results for the same parameters as Fig. 4(b) except for the scattering albedo of the first layer. The parameters are: $n_1 = 1.5$, $n_2 = 3$, $\tau_1 = \tau_2 = 1$, $\widetilde{q}^{\mathrm{r}}_{S_{-\infty}} = 1.0^4$, $\widetilde{q}^{\mathrm{r}}_{S_{+\infty}} = 0.25^4$, $N_1 = N_2 = 0.0625$, $H_1 = H_2 = 1$, $\widetilde{T}_{g1} = 1$, $\widetilde{T}_{g2} = 0.25$, $\delta = 0.5$, and $C_{21} = 1$. As shown in Fig. 4, the results of this paper are almost the same as the exact numerical solution in [9] so that it is difficult to distinguish both the curves without scattering and with scattering. Whereas the approximate results in [10] deviate a little from the results in [9]. This demonstrates that the equations obtained here are correct and the accuracy of the method developed is high because the space solid angle is not dispersed but is directly integrated.

Table 1
Comparison of the results in this paper with those in [8] ($N_1 = N_2 = N$)

N	τ_1	τ_2	ω_1	ω_2	X						$\widetilde{q}_t$	
					$\widetilde{T}$ [8]			$\widetilde{T}$ (This paper)			[8]	This paper
					0.25	0.5	0.75	0.25	0.5	0.75		
1.0			0	0	0.6402	0.7693	0.8849	0.64030	0.76938	0.88503	2.3788	2.37876
	2.4	0.6	0	0.95	0.6393	0.7672	0.8836	0.63939	0.76741	0.88372	2.3640	2.36416
			0.95	0	0.6321	0.7613	0.8828	0.63215	0.76146	0.88282	2.3284	2.32824
			0	0	0.8023	0.9097	0.9409	0.80241	0.90983	0.94084	0.3252	0.32500
	2.4	0.6	0	0.95	0.8006	0.9065	0.9469	0.80069	0.90669	0.94705	0.3220	0.32204
			0.95	0	0.7693	0.9029	0.9427	0.76938	0.90301	0.94265	0.3148	0.31488
0.01			0	0	0.7556	0.8440	0.9103	0.75557	0.84395	0.91026	0.3184	0.31832
	1.5	1.5	0	0.95	0.7535	0.8410	0.9114	0.75346	0.84103	0.91144	0.3144	0.31424
			0.95	0	0.7140	0.8430	0.9130	0.71407	0.84304	0.91293	0.3100	0.30992
			0	0	0.6957	0.7650	0.8790	0.69546	0.76493	0.87868	0.3144	0.31432
	0.6	2.4	0	0.95	0.6937	0.7679	0.8763	0.69364	0.76786	0.87625	0.3096	0.30956
			0.95	0	0.6489	0.7664	0.8815	0.64875	0.76637	0.88132	0.3088	0.30872

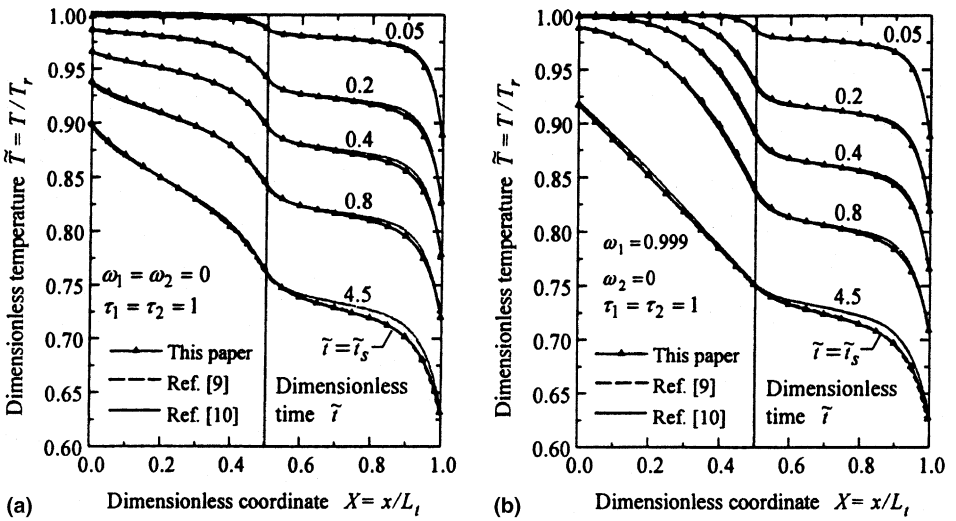

Fig. 4. Comparison of present results with those of [9,10]: (a) without scattering in both of the layers; (b) isotropic scattering in the first layer.

5. Results and analysis

Effects of scattering albedo of the composite, reflective characteristics of the surfaces, emissivities of surface S_2 and conduction–radiation parameter on temperature and flux are considered. The spectral band models shown in Table 2 are used to simulate the spectral properties of the composite.

Table 2
Spectral band model for the composite

k	Spectrum A			Spectrum B		
	λ	κ_k	ω_k	λ	κ_k	ω_k
1	0–2	2.0	0.95	0–2	5.0	0.0
2	2–5	0.2	0.95	2–5	0.5	0.0
3	5–∞	Opaque		5–∞	Opaque	

5.1. Effects of reflective characteristics and single-scattering albedo

$P_{ref} = 1$ for the specular surface, $P_{ref} = 0$ for the diffuse surface, and $P_{ref} = 0.3$ and $P_{ref} = 0.7$ for the combined specular and diffuse reflective surface are adopted. The reflectivities of a semitransparent surface are calculated by using Fresnel's equations, and the emissivities of opaque surface S_2 are $\varepsilon_{2g} = \varepsilon_{g2} = 0.4$. The composite is assumed to be gray, and the optical thickness is kept constant, $\tau_1 = 0.1$ and $\tau_2 = 5$. The following three conditions of the scattering albedo are considered: $\omega_1 = \omega_2 = 0$ (see Fig. 5(a)), $\omega_1 = 0.99$ and $\omega_2 = 0$ (see Fig. 5(b)), $\omega_1 = 0$ and $\omega_2 = 0.99$ (see Fig. 5(c)), and $\omega_1 = 0.99$ and $\omega_2 = 0.99$ (see Fig. 5(d)). The boundaries are subjected to radiative and convective heat transfer, and $\widetilde{q}^{r}_{S_{-\infty}} = 1.5^4$, $\widetilde{q}^{r}_{S_{+\infty}} = 0.5^4$, $\widetilde{T}_{g1} = \widetilde{T}_{g2} = 1.0$, $H_1 = H_2 = 5$. The other parameter are: $n_1 = 1.5$, $n_2 = 3.0$, $N_1 = N_2 = 0.025$, $\delta = 0.5$, $C_{21} = 1$.

As shown in Fig. 5,

1. Since radiative energy of the surroundings can be directly transferred into the interior of STM, and radiant propagation is more rapid than conduction, and the optical thickness of the first layer is smaller compared to that of the

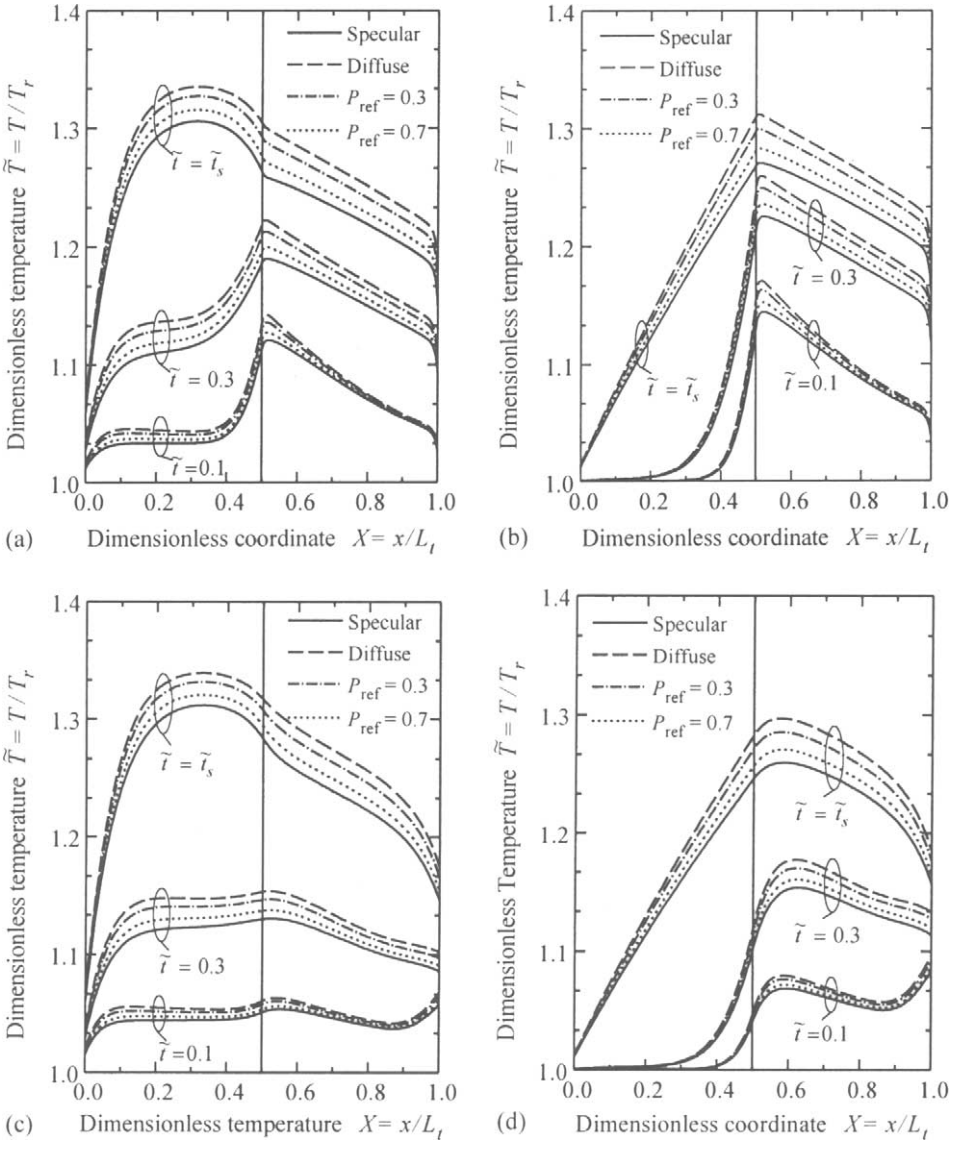

Fig. 5. Effects of scattering and reflective characteristic on temperature distribution: (a) $\omega_1 = \omega_2 = 0$; (b) $\omega_1 = 0.99$, $\omega_2 = 0$; (c) $\omega_1 = 0$, $\omega_2 = 0.99$; (d) $\omega_1 = 0.99$, $\omega_2 = 0.99$.

second layer; the peak value of transient temperature appears within the second layer and near the internal interface, and even two peak values of temperature appear within the composite for the small dimensionless time $\widetilde{t} = 0.1$.

2. For the steady state, the peak value of temperature in the second layer disappears due to the effect of conduction, but that in the first layer still exists (see Fig. 5(a)), which is the same as that for a two-layer STM with both semitransparent boundaries [15].
3. Since the optical thickness is kept constant, when $\omega_1 = 0.99$, the absorbing optical thickness of the first layer becomes 0.001, so that the peak value of temperature appears within the second layer for both transient state and steady state (see Fig. 5(b)).
4. When $\omega_1 = 0$ and $\omega_2 = 0.99$, compared with Fig. 5(a), the peak value and the gradient of temperature for transient state minish.
5. From Figs. 5(a)–(d), we can see that the reflective characteristics affect only the value of temperature, but not the trend of temperature distribution. Furthermore, for the combined specular and diffuse reflection, the temperature distribution falls between those for specular and diffuse reflection. In addition, for all reflective characteristics, the temperature distribution trends are the same when the other parameters are same.

5.2. Effect of conduction–radiation parameter

To show the effect of conduction–radiation parameter N_b on the steady-state temperature distribution and heat flux density for gray composite with the specular reflection, five groups of N are adopted, i.e.,

(a) $N_1 = N_2 = 0.025$ (solid line);
(b) $N_1 = 0.25$, $N_2 = 0.025$ (dash line);
(c) $N_1 = 2.5$, $N_2 = 0.025$ (double dot–dash line);
(d) $N_1 = 0.025$, $N_2 = 0.25$ (dot–dash line);
(e) $N_1 = 0.025$, $N_2 = 2.5$ (dot line).

No scattering, $\omega_1 = \omega_2 = 0$, $\tau_1 = 0.5$, $\tau_2 = 0.1$; first kind boundary conditions at both boundaries, $\widetilde{T}_{S_1} = 1$, $\widetilde{T}_{S_2} = 0.5$. The other parameters are the same as those of Figs. 5(a)–(d).

Fig. 6 and Table 3 provide the temperature distributions and heat flux densities, respectively. Compared with condition (a), when the conduction–radiation parameter of the first layer N_1 increases and that of the second layer N_2 remains unchanged. Due to higher conduction in the first layer, the temperature gradient in the first layer falls and that in the second layer rises, and the radiative heat flux density decreases and the conductive heat flux density increases. When N_1 remains the same, but N_2 increases, the change of the temperature gradient in the composite is contrary to that for conditions (b) and (c).

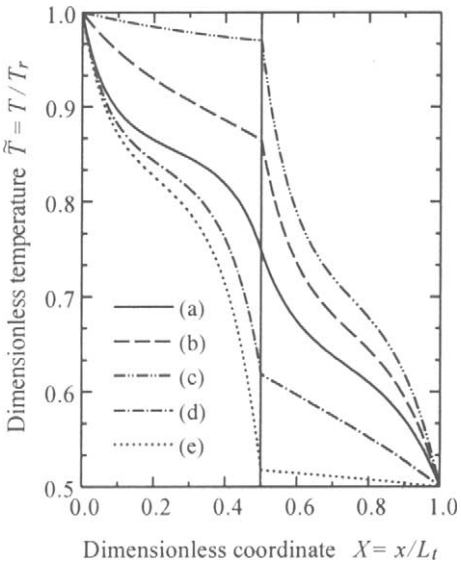

Fig. 6. Effects of conduction–radiation parameter on temperature distribution.

Table 3
Dimensionless heat fluxes under the condition of Fig. 6

	Case (a)	Case (b)	Case (c)	Case (d)	Case (e)
$\widetilde{q}^{\mathrm{r}}$	0.4125	0.3120	0.1972	0.4567	0.4848
$\widetilde{q}^{\mathrm{cd}}$	0.2053	0.5132	0.8732	0.2314	0.2486
$\widetilde{q}^{\mathrm{t}}$	0.6178	0.8252	1.0705	0.6880	0.7334

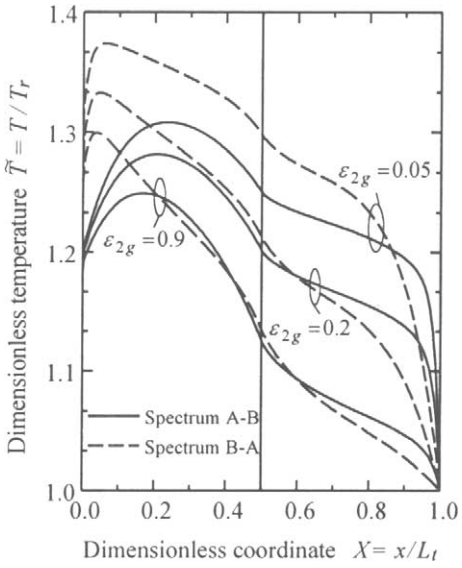

Fig. 7. Effects of inner surface emissivity ε_{2g} on temperature distribution.

5.3. Effect of emissivity of opaque surface

Fig. 7 shows the effect of the emissivity of opaque boundary surface S_2 on the temperature distribution and the heat flux density for the two-layer STM with the diffuse reflective surfaces. The spectral band models shown in Table 2 are adopted to simulate the spectral properties of the composite, $L_1 = L_2 = 1$, $C_{21} = 1$. The mixed boundary conditions are used, i.e., a third kind boundary condition for surface S_1, $H_1 = 2$, $\widetilde{T}_{g1} = 1$, $\widetilde{q}^{\mathrm{r}}_{S_{-\infty}} = 1.5^4$; and a first kind for surface S_2, $\widetilde{T}_{S_2} = 1$. ε_{2g} is equal to 0.05, 0.2, and 0.9, respectively. And each ε_{2g} corresponds two kinds of conditions, i.e.,

(a) spectral band model A and model B are applied to the first and second layer, respectively (Spectrum A–B);
(b) spectral band model A and model B are applied to the second and the first layer, respectively (Spectrum B–A).

As shown in Fig. 7, with the increase of ε_{2g}, the reflectivity $\rho_{2g} = 1 - \varepsilon_{2g}$ decreases so that the temperature in the composite falls. For conditions (a) and (b), the peak values of temperature appear in the first layer. But, compared with the spectral band model B, the optical thickness of model A is smaller and has strong isotropic scattering. So, the peak value of temperature for condition (a) appears somewhere closer to boundary surface S_1 than that for condition (b).

6. Conclusions

On the basis of our previous work, the ray tracing method in combination with Hottel's zonal method is extended to the study of the transient coupled radiation and conduction in a two-layer isotropically scattering STM with one semitransparent outer boundary and one opaque outer boundary. It needs only to disperse the space position, but rather than disperse the solid angle. The composite radiative properties are modeled by two spectral band models, and the reflectivities of a semitransparent surface are obtained by Fresnel's equation. The comparison with the results of [8–10] shows that the present results are accurate. On this basis, the effects of single-scattering albedo, reflective characteristics, conduction–radiation parameter, and emissivity on the temperature distribution and heat flux are investigated.

By analyzing of the present results, the following conclusions are drawn:

1. For a two-layer STM with different radiative properties, one semitransparent outer boundary and one opaque outer boundary, the peak value of temperature may appear in the composite, and may be two peak values of temperature for a small dimensionless time.
2. An inhomogeneous STM can be an equivalent to a composite composed of the impinging multi-layer STM. When the composite is subjected to high-temperature surroundings at one semitransparent boundary and low-temperature surroundings at another boundary, we can predict that the peak value or maximum of the transient and steady-state temperature may nevertheless appear inside the media.

Acknowledgements

This research is supported by the Chinese National Science Fund for Distinguished Young Scholars (No. 59725617), the National Natural Science Foundation of China (No. 59806003).

Appendix A. Expressions and reciprocity relationships of RTC equations for diffuse reflection

A.1. RTC for an absorbing, emitting composite medium

For diffuse reflection, two rays with different launching angles can be mixed. So, in this paper, the RTC for diffuse reflection are obtained by tracing the radiative energy using DRTC. The DRTCs are given as:

$$(s_b s_P)_k = 2E_3(\kappa_{b,k} L_b), \tag{A.1}$$

$$(s_1 v_{1_j})_k = 2E_3(\kappa_{1,k} x_{S_1,1_j}) - 2E_3(\kappa_{1,k} x_{S_1,1_{j+1}}), \tag{A.2}$$

$$(s_P v_{2_j})_k = 2E_3(\kappa_{2,k} x_{S_P,2_j}) - 2E_3(\kappa_{2,k} x_{S_P,2_{j+!}}), \tag{A.3}$$

$$(s_2 v_{2_j})_k = 2E_3(\kappa_{2,k} x_{S_2,2_{j+1}}) - 2E_3(\kappa_{2,k} x_{S_2,2_j}), \tag{A.4}$$

$$(s_P v_{1_j})_k = 2E_3(\kappa_{1,k} x_{S_P,1_{j+1}}) - 2E_3(\kappa_{1,k} x_{S_P,1_j}), \tag{A.5}$$

$$(v_{b_i} v_{b_j})_k = 2E_3(\kappa_{b,k} x_{b_{i+1},b_j}) - 4E_3(\kappa_{b,k} x_{b_i,b_j}) + 2E_3(\kappa_{b,k} x_{b_i,b_{j+1}}) \quad (i \neq j), \tag{A.6}$$

$$(v_{b_i} v_{b_j})_k = 4\kappa_{b,k}\Delta x - 2[1 - 2E_3(\kappa_{b,k}\Delta x)] \quad (i = j). \tag{A.7}$$

For convenience's sake, two functions are defined here [16]

$$FM_{b,k} = \rho_{bP}\rho_{bg}(s_b s_P)_k^2, \tag{A.8}$$

$$FM_k = \gamma_{1P}\gamma_{2P}\rho_{1g}\rho_{2g}(s_1 s_P)_k^2 (s_2 s_P)_k^2 / [(1 - FM_{1,k})(1 - FM_{2,k})]. \tag{A.9}$$

RTC equations are obtained by tracing the radiative energy using DRTC.

$$(S_{-\infty} S_2)_k^{\mathrm{d}} = \frac{\gamma_{g1}\gamma_{1P}\varepsilon_{2g}(s_1 s_P)_k (s_P s_2)_k}{(1 - FM_{1,k})(1 - FM_{2,k})(1 - FM_k)} \tag{A.10}$$

$$(S_{-\infty} S_{-\infty})_k^{\mathrm{d}} = \rho_{g1} + \frac{\gamma_{g1}\gamma_{1g}\rho_{1P}(s_1 s_P)_k^2}{1 - FM_{1,k}} + \frac{\gamma_{g1}\gamma_{1g}\gamma_{1P}\rho_{2g}\gamma_{2P}(s_1 s_P)_k^2 (s_2 s_P)_k^2}{(1 - FM_{1,k})^2 (1 - FM_{2,k})(1 - FM_k)}, \tag{A.11}$$

$$(S_2 S_2)_k^{\mathrm{d}} = \frac{\varepsilon_{2g}\varepsilon_{2g}\rho_{2P}(s_2 s_P)_k^2}{1 - FM_{2,k}} + \frac{\varepsilon_{2g}\varepsilon_{2g}\gamma_{2P}\rho_{1g}\gamma_{1P}(s_2 s_P)_k^2 (s_1 s_P)_k^2}{(1 - FM_{2,k})^2 (1 - FM_{1,k})(1 - FM_k)}, \tag{A.12}$$

$$(S_{-\infty} V_{1_j})_k^{\mathrm{d}} = \frac{(s_1 v_{1_j})_k + (s_1 s_P)_k \rho_{1P}(s_P v_{1_j})_k}{(1 - FM_{1,k})/\gamma_{g1}} + \frac{(s_1 s_P)_k (s_P s_2)_k^2 [(s_P v_{1_j})_k + (s_P s_1)_k \rho_{1g}(s_1 v_{1_j})_k]}{(1 - FM_{1,k})^2 (1 - FM_{2,k})(1 - FM_k)/\gamma_{g1}\rho_{2g}\gamma_{1P}\gamma_{2P}}, \tag{A.13}$$

$$(S_{-\infty} V_{2_j})_k^{\mathrm{d}} = \frac{\gamma_{g1}\gamma_{1P}(s_1 s_P)_k [(s_P v_{2_j})_k + (s_P s_2)_k \rho_{2g}(s_2 v_{2_j})_k]}{(1 - FM_{1,k})(1 - FM_{2,k})(1 - FM_k)}, \tag{A.14}$$

$$(S_2V_{1_j})_k^{\mathrm{d}} = \frac{\varepsilon_{2g}\gamma_{2P}(s_2s_P)_k\left[(s_Pv_{1_j})_k + (s_Ps_1)_k\rho_{1g}(s_1v_{1_j})_k\right]}{(1-FM_{1,k})(1-FM_{2,k})(1-FM_k)}, \tag{A.15}$$

$$(S_2V_{2_j})_k^{\mathrm{d}} = \frac{(s_2v_{2_j})_k + \rho_{2P}(s_2s_P)_k(s_Pv_{2_j})_k}{(1-FM_{2,k})/\varepsilon_{2g}} + \frac{(s_2s_P)_k(s_1s_P)_k^2\left[(s_Pv_{2_j})_k + (s_Ps_2)_k\rho_{2g}(s_2v_{2_j})_k\right]}{(1-FM_{2,k})^2(1-FM_{1,k})(1-FM_k)/\varepsilon_{2g}\gamma_{2P}\rho_{1g}\gamma_{1P}}, \tag{A.16}$$

$$\begin{aligned}(V_{b_i}V_{b_j})_k^{\mathrm{d}} = {} & (v_{b_i}v_{b_j})_k + \frac{(s_bv_{b_i})_k\rho_{bg}\left[(s_bv_{b_j})_k + (s_bs_P)_k\rho_{bP}(s_Pv_{b_j})_k\right]}{(1-FM_{b,k})} + \frac{(s_Pv_{b_i})_k\rho_{bP}\left[(s_Pv_{b_j})_k + (s_bs_P)_k\rho_{bg}(s_bv_{b_j})_k\right]}{(1-FM_{b,k})} \\ & + \frac{\left[(s_bv_{b_i})_k\rho_{bg}(s_bs_P)_k\gamma_{bP} + (s_Pv_{b_i})_k\gamma_{bP}\right]\rho_{cg}\gamma_{cP}(s_cs_P)_k^2\left[(s_Pv_{b_j})_k + (s_bs_P)_k\rho_{bg}(s_bv_{b_j})_k\right]}{(1-FM_{b,k})^2(1-FM_{c,k})(1-FM_k)},\end{aligned} \tag{A.17}$$

$$(V_{1_i}V_{2_j})_k^{\mathrm{d}} = \frac{\left[(s_1v_{1_i})_k\rho_{1g}(s_1s_P)_k\gamma_{1P} + (s_Pv_{1_i})_k\gamma_{1P}\right]\left[(s_Pv_{2_j})_k + (s_2s_P)_k\rho_{2g}(s_2v_{2_j})_k\right]}{(1-FM_{1,k})(1-FM_{2,k})(1-FM_k)}. \tag{A.18}$$

A.2. Reciprocity relationships of RTC equations

For diffuse reflection, the total reflection is considered in the reflectivity and transmissivity, so the transmissivity and reflectivity of the different sides of an interface are different. The reciprocity relationships of RTC equations are given by

$$\begin{aligned}&(S_{-\infty}S_2)_k^{\mathrm{d}}\gamma_{2P}\gamma_{1g} = (S_2S_{-\infty})_k^{\mathrm{d}}\gamma_{1P}\gamma_{g1}, && (S_{-\infty}V_{1_i})_k^{\mathrm{d}}\gamma_{1g} = (V_{1_i}S_{-\infty})_k^{\mathrm{d}}\gamma_{g1},\\ &(S_{-\infty}V_{2_j})_k^{\mathrm{d}}\gamma_{2P}\gamma_{1g} = (V_{2_j}S_1)_k^{\mathrm{d}}\gamma_{1P}\gamma_{g1}, && (S_2V_{1_j})_k^{\mathrm{d}}\gamma_{1P} = (V_{1_j}S_2)_k^{\mathrm{d}}\gamma_{2P},\\ &(S_2V_{2_j})_k^{\mathrm{d}} = (V_{2_j}S_2)_k^{\mathrm{d}}, && (V_{1_i}V_{2_j})_k^{\mathrm{d}}\gamma_{2P} = (V_{2_j}V_{1_i})_k^{\mathrm{d}}\gamma_{1P},\\ &(V_{1_i}V_{1_j})_k^{\mathrm{d}} = (V_{1_j}V_{1_i})_k^{\mathrm{d}}, && (V_{2_i}V_{2_j})_k^{\mathrm{d}} = (V_{2_j}V_{2_i})_k^{\mathrm{d}}.\end{aligned} \tag{A.19}$$

References

[1] H.P. Tan, M. Lallemand, Transient radiative–conductive heat transfer in flat glasses submitted to temperature, flux and mixed boundary conditions, Int. J. Heat Mass Transfer 32 (5) (1989) 795–810.

[2] R.E. Field, R. Viskanta, Measurement and prediction of the dynamic temperature distributions in soda lime glass plates, Am. Ceram. Soc. 73 (7) (1990) 2047–2053.

[3] J.R. Thomas Jr., Coupled radiation/conduction heat transfer in ceramic liners for diesel engines, Num. Heat Transfer, Part A 21 (1992) 109–122.

[4] Z. Yin, Y. Jaluria, Zonal method to model radiative transport in an optical fiber drawing furnace, J. Heat Transfer 119 (1997) 597–603.

[5] S.H. Park, C.L. Tien, Radiation induced ignition of solid fuels, Int. J. Heat Mass Transfer 33 (1990) 1511–1520.

[6] R. Viskanta, E.E. Anderson, Heat transfer in semi-transparent solids, in: Advances in Heat Transfer, vol. 11, Academic Press, New York, 1975, pp. 317–441.

[7] C.H. Ho, M.N. Özisik, Combined conduction and radiation in a two-layer planar medium with flux boundary condition, Num. Heat Transfer 11 (1987) 321–340.

[8] C.H. Ho, M.N. Özisik, Simultaneous conduction and radiation in a two-layer planar medium, J. Thermophys. Heat Transfer 1 (2) (1987) 154–161.

[9] C.M. Spuckler, R. Siegel, Refractive index and scattering effects on radiation in a semitransparent laminated layer, J. Thermophys. Heat Transfer 8 (2) (1994) 193–201.

[10] R. Siegel, Green's function and two-flux analysis for transient radiative transfer in a composite layer, in: Proceedings of the National Heat Transfer Conference, vol. 325, ASME HTD-Vol.325, 1996, pp. 35–43.

[11] R. Siegel, Temperature distribution in a composite of opaque and semitransparent spectral layers, J. Thermophys. Heat Transfer 11 (4) (1997) 533–539.

[12] R. Siegel, Transient thermal analysis of parallel translucent layers by using Green's functions, J. Thermophys. Heat Transfer 13 (1) (1999) 10–17.

[13] H.P. Tan, L.M. Ruan, X.L. Xia, Q.Z. Yu, T.W. Tong, Transient coupled radiative and conductive heat transfer in an absorbing, emitting, and scattering medium, Int. J. Heat Mass Transfer 42 (15) (1999) 2967–2980.

[14] H.C. Hottel, A.F. Sarofim, Radiative Transfer, McGraw-Hill, New York, 1967, pp. 265–266.

[15] H.P. Tan, P.Y. Wang, X.L. Xia, Transient coupled radiation and conduction in an absorbing and scattering composite layer, J. Thermophys. Heat Transfer 14 (1) (2000) 77–87.

[16] P.Y. Wang, H.P. Tan, L.H. Liu, T.W. Tong, Coupled radiation and conduction in a scattering composite layer with coatings, J. Thermophys. Heat Transfer 14 (4) (2000) 512–522.
[17] R. Siegel, J.R. Howell, Thermal Radiation Heat Transfer, third ed., Hemisphere, Washington, DC, 1992, pp. 23, 33, 115.
[18] J.C. Richmond, Relation of emittance to other optical properties, J. Res. Nat. Bur. Stand. C 67 (3) (1963) 217–226.